Adaptive characterization of laser damage from sparse defects

Sam Richman*, Alexander R. Martin, Quentin Turchette and Trey Turner
REO, 5505 Airport Blvd., Boulder, CO, USA 80301

ABSTRACT

Standard techniques for characterizing laser damage are ill-suited to the regime in which sparse defects form the dominant damage mechanism. Previous work on this problem using REO's automated laser damage threshold test system has included linking damage events in HfO_2/SiO_2 high reflector coatings with visible pre-existing defects, and using a probability per defect based on size and local fluence to generate predictions of damage events in subsequent coating runs. However, in all this work the test sites were always in a predefined array, and the association of defects with damage events was done only after the fact. In an effort to make this process both more efficient and less susceptible to uncertainties, we have now developed an adaptive test strategy that puts defect identification and analysis into the loop. A map of defect locations and sizes on a test surface is compiled, and a set of test sites and corresponding fluences based on that map is then generated. With defects of interest now centered on the damaging beam, the problem of higher-order spatial variation in the beam profile is greatly reduced. Test sites in zones with no detectable defects are also included. This technique allows for the test regimen to be tailored to the specific surface under consideration. We report on characterization of a variety of coating materials and designs with this adaptive method.

Keywords: Laser damage threshold, LDT, HLDT, damage testing, surface quality, inspection

1. INTRODUCTION

It has been established since the early days of the field that defects can serve as initiators of laser-induced damage[1]. Sparsely-distributed defects at or near the surfaces of optical components pose a special problem for characterization of laser damage behavior. Testing in accordance with the ISO 21254 standard[2] using as few as 10 widely separated test sites at a given fluence can give a very incomplete picture about how the optic might function in actual use. In this regime the effect of beam size can be considerable[3]. Various methods have been implemented to address this phenomenon, including scanning of the damaging beam over a wide area as is done with the NIF MEL01-013-0D test protocol[4].

However, when laser damage is governed by sparse defects there is also an opportunity to anticipate such behavior via nondestructive testing. Recent work at REO has focused on the prospect of predicting damage probabilities of production optics by mapping the size and areal density distribution of defects with automated dark field microscopy[5,6]. This is a natural extension of REO's thrust more generally to automate surface quality inspection[7,8]. These prior efforts demonstrated a strong link between damage events and visible pre-existing defects, and indicated the possibility of predicting damage in a statistical sense. However, they were limited in the following ways:

1) Uncertainty in the knowledge of beam location and profile led to uncertainty in the calculation of local fluence at a particular defect.
2) Damage events whose spatial extent is large compared to typical inter-defect spacing (covering multiple defects) are not easily attributed to a single defect. As such only comparatively low fluences (<30 J/cm^2) were studied in detail, in order to limit the size of damage events.
3) Only high-reflector (HR) coatings were studied.
4) Only HfO_2 and SiO_2 were used as coating materials.

In this paper we describe a novel measurement technique designed to address points (1) and (2). We also report results on HR and anti-reflector (AR) coatings using both HfO_2/SiO_2 and Nb_2O_5/SiO_2 material sets, as a way to begin to expand beyond points (3) and (4).

* SamR@reoinc.com; phone 1-303-245-4337; fax 1-303-447-3279; www.reoinc.com

Laser-Induced Damage in Optical Materials: 2014, edited by Gregory J. Exarhos, Vitaly E. Gruzdev, Joseph A. Menapace, Detlev Ristau, MJ Soileau, Proc. of SPIE Vol. 9237, 923718 · © 2014 SPIE · CCC code: 0277-786X/14/$18 · doi: 10.1117/12.2068213

2. INSTRUMENTATION AND METHODOLOGY

2.1 Test system

The basic hardware layout of the test station used for both defect identification and damage testing has been described elsewhere[9]; a schematic is shown in Figure 1. Images are acquired with an 8-bit camera via a microscope with a 5x objective and have a 1.65 mm x 1.65 mm field of view. Illumination is provided by white LED light delivered via fibers and pointed at a shallow angle to the sample. The samples are irradiated with a Q-switched, flashlamp-pumped Nd:YAG laser operating at 1064 nm, with pulsewidth = 25 ns and PRF = 20 Hz. The size of the elliptical, focused spot at the surface of the device under test is 0.60 mm x 0.38 mm (at the $1/e^2$ points). This smaller spot size compared to previous versions of the instrument allows for a maximum fluence at the sample of about 150 J/cm^2. The system incorporates an energy meter, temporal profiling photodetector, and spatial profiling camera. A motorized X-Y stage shifts samples between the microscope inspection and laser irradiation positions of the instrument with ±5 μm repeatability.

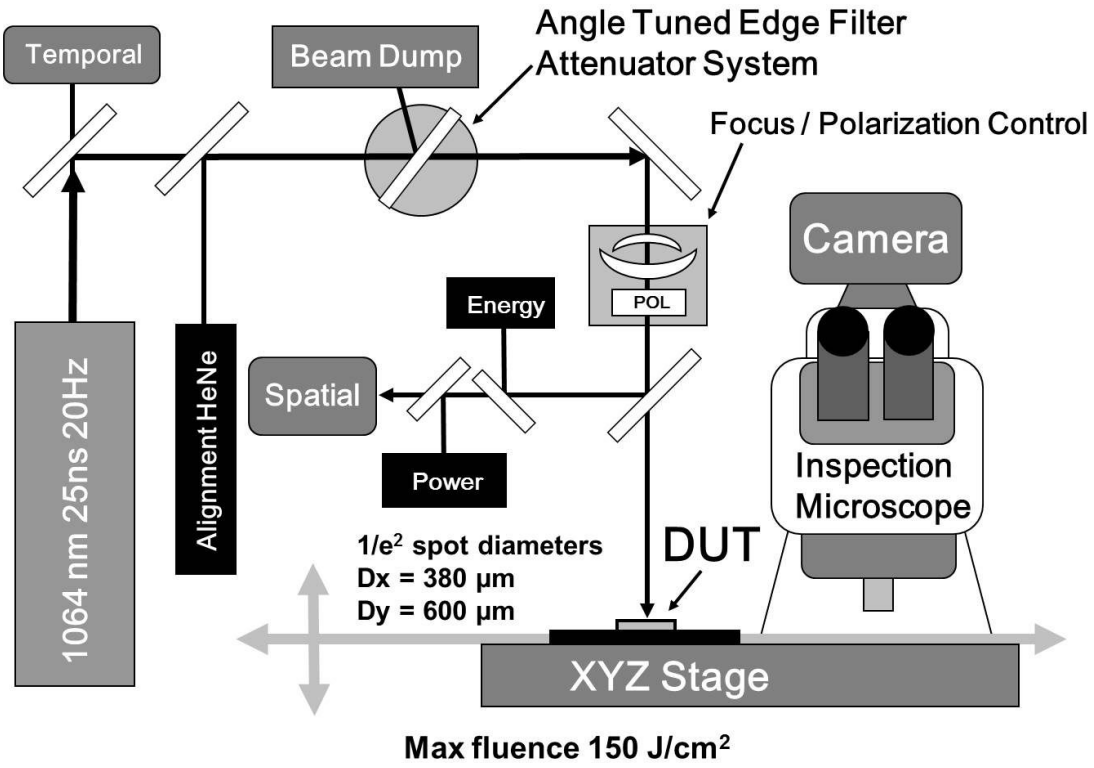

Figure 1. Schematic diagram of laser damage test system.

The "Find and Zap Defects" (FAZ) protocol identifies defects on the test surface and then chooses test sites based on the location of these defects. Fluences at the defect locations can be assigned arbitrarily. In this sense it is adaptive – the test sites that are actually chosen are dependent upon the distribution of defects of that optic. Each step in the process is outlined in more detail in the following subsections. Note that the whole process is automated with the exception of the damage identification and sizing, though in principle this could be automated as well - and in fact has been for other test protocols used with the REO system, like the NIF MEL01-013-0D.

2.2 Take survey photos

The first step is to take survey photos covering the entire clear aperture of the sample. For the 2" diameter optics in this study, this comprises 437 contiguous images in a rectangular grid. The camera exposure time for each image is 1000 ms; longer exposures do not increase the signal-to-background ratio of the smallest discernible defects.

2.3 Identify defects

The survey images are then analyzed automatically via MATLAB code running on the test computer. A cluster of four or more contiguous pixels that exceed a pre-defined brightness threshold is flagged as a defect. The size of the defect is defined as the square root of its area; the minimum size defect is 2.3 μm. A list of all defects on the sample along with their sizes and coordinates is generated.

2.4 Create test site list

From the defect list the code then generates a test site list. Before the survey images are taken, the user has already set some initial parameters for the site list selection algorithm. These parameters include the test fluences, weighting factors that govern the fraction of defects of a given size to be tested at each fluence, and an exclusion diameter that defines the size of a test site. The exclusion diameter restricts the test site to either a single defect at the center of the beam or no defect at all. The exclusion diameter was typically set to be 1.2 mm, which for the 0.60 mm x 0.38 mm spot size means that at a nominally no-defect test site the highest possible fluence at a nearby visible defect is only about 1% of the peak fluence. The parameters do allow for a very skewed number of test sites as a function of defect size and fluence if desired, but typically the tests were run with a wide, even fluence distribution that was independent of defect size. This helps to avoid biases in the data based on actual variations in defects from part-to-part within a coating run.

2.5 Take "before" photos

A set of before-irradiation images is then taken, one at each test site. In these images, the target defect now appears at the center of the FOV; in the case of the nominally no-defect sites there are no above-threshold defects within a circle defined by the exclusion diameter. While these images are not used systematically in the analysis of damage, they do help verify the functioning of the system.

2.6 Irradiate test sites

Test sites are irradiated by the damaging laser beam at the specified fluence. In this study, each site was irradiated for 1 s or about 20 pulses. All test sites at a given fluence setting are imaged again directly prior to exposure, though like the before photos of the previous section this is only to check for system functioning and help diagnose any problems.

2.7 Take "after" photos

Images after laser irradiation are taken at each test site, with an effective exposure time reduced to 125 ms to avoid excessive brightness and pixel saturation from the sometimes quite large damage events.

2.8 Evaluate damage

This is the only step of the process that requires manual intervention. An operator is presented with a series of the before and after images at each test site. For each after image, the operator decides whether or not damage has occurred. If it has, then the operator defines the location and size of the damage event. Although the size information was not used in later analysis, the location of the damage events was initially monitored as a check on the colocation of the damaging beam and camera FOV on any given test site.

2.9 Perform analysis

The data are then reduced. The basic output of the analysis is a three-dimensional map of the probability of damage as a function of both fluence and size of defect.

3. TEST SAMPLES

All samples in this study were coated optics using 2" diameter fused silica plane-parallel substrates, with surface quality equal to or better than 20-10 as judged by MIL-PRF-13830B. The polishing and pre-coating cleaning were done with processes normally used to manufacture high laser damage threshold components. All coatings were performed in the same ion beam sputtering (IBS) chamber. This chamber was not maintained on the same schedule as a standard production chamber and as a result the overall defect density on the samples is somewhat higher than production optics. Table 1 summarizes the four sets of optics tested with the FAZ protocol. The HR coatings had $R > 99.95\%$, and the AR coatings $R < 0.03\%$, both at 1064 nm, 0° AOI. Set #1 comprised two separate coating runs to increase the sample size,

but there was no discernible difference in the damage statistics between parts from the two runs. Nb_2O_5, with a bandgap of 3.4 eV, was chosen as an easily-damaged contrast to HfO_2 (bandgap of 5.3 eV) which is commonly used as the high-index material in high laser damage threshold coatings. The coating design of the Set #3 Nb_2O_5 HR (28 layers) was chosen to match the reflectivity of the Set #1 HfO_2 HR (40 layers).

Table 1. Summary of test optics.

Set #	# Parts	Coating type	Coating thickness (μm)	Material set	# Test sites
1	12	HR	6.4	HfO_2/SiO_2	4552
2	8	AR	0.45	HfO_2/SiO_2	2111
3	6	HR	4.2	Nb_2O_5/SiO_2	1899
4	9	AR	0.43	Nb_2O_5/SiO_2	2530

Between the four sets, the 35 parts encompass a total of 11,092 test sites and 4,392 damage events.

4. RESULTS

4.1 Defect distributions

The first step in the testing is characterization of the defects on the sample under test. Figure 2 is a histogram of areal number densities of defects from one of the Set #1(HfO_2/SiO_2 HR) optics as determined from the survey images of that part. Defect densities are plotted as a function of defect size in equal width bins of 5 μm. The first size bin starts at 2.3 μm, which is the smallest size defined by the detection criteria. The total density of defects larger than 2.3 μm on this optic is 0.99/mm^2.

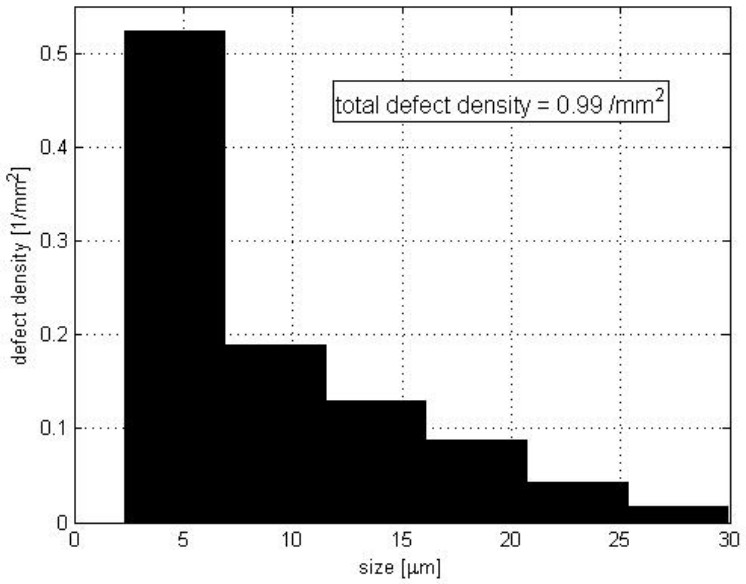

Figure 2. Defect size distribution of one of the Set #1 optics (HfO_2/SiO_2 HR).

A similar plot for one of the Set #2 optics (HfO_2/SiO_2 ARs) is shown in Figure 3. Note that the overall density of defects, 0.15/mm^2, is less than in the case of the Set #1 optics, and also the distribution is skewed more toward smaller defects.

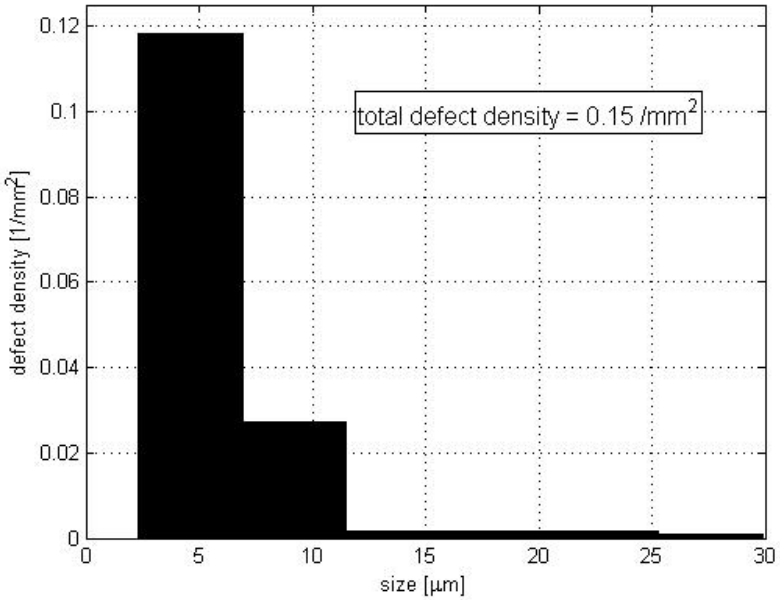

Figure 3. Defect size distribution of one of the Set #2 optics (HfO_2/SiO_2 AR).

The larger number and size of defects in HR coatings compared to AR is also evident with the Nb_2O_5/SiO_2 material set. One possible cause is that the defects are predominately created during the deposition, as the HR coating runs are several times longer than the AR runs and thus afford more opportunities to create defects. Another possible cause is that these defects grow as nodules[10] from seeds that are smaller than the 2.3 μm visibility limit. Note that the FAZ technique is in principle insensitive to the actual distribution of visible defects on the sample, because all the probabilities are calculated per defect. However, this only holds true to the extent that the effect of defects smaller than the visibility limit is negligible.

As a rudimentary test for the existence of smaller defects, two optics each from Set #1 and Set #2 were inspected with a more sensitive microscope and image acquisition system. The higher resolving power of the microscope and lower noise floor of the camera allow for the detection of defects down to 0.7 μm. Only a small fraction of the surface area of each optic was inspected, so the data are far from complete. However, it was clear that the trend toward increasing density of defects of smaller size in both the Set #1 HR optics and Set #2 AR optics continues in the size range 0.7-2.3 μm.

4.2 Damage probability maps

The results from the testing of Set #1 optics (HfO_2/SiO_2 HRs) are shown in Figure 4. Fluence is given along the x-axis, binned in equal intervals of 15 J/cm^2. The y-axis is the size of the defect probed, where the size of the bins has been chosen to give roughly equal numbers of defects in the two intermediate bins. The top-most bin represents very large defects, and there are fewer of these on the optics. The bottom-most bin, labeled "not visible", represents the test sites with no defects visible with the inspection equipment. The color scale encodes the probability of damage, and the number of sites tested for a given fluence and size is shown on each block. The red trace in the lower graph comes from summing events over the top three defect size bins (the visible defects); the blue trace comes from the lowest (no visible defects) bin. At each data point the error bars represent a 95% confidence interval.

Unsurprisingly, damage probability increases monotonically (within statistical variations) with fluence and size of defect. As we have seen in previous work, there is little evidence for any meaningful threshold-like behavior for damage initiated by defects on these scales; the probability rises steadily from the lowest fluence bin. The curve for no visible defects has a more threshold-like behavior starting above 45 J/cm^2, though it still rises only slowly above that point. However, there is a wide range of fluences – at least between 15 J/cm^2 and 75 J/cm^2 (an important region for producers and consumers of high laser damage threshold optics) – for which there is signficant separation of the damage probability curves for the visible defect and no visible defect cases. This separation allows for the visible defects to be

approximated as the sole damage initiators, making damage prediction from a defect map possible. Figure 5 shows the same probability map for Set #2 optics (HfO_2/SiO_2 ARs).

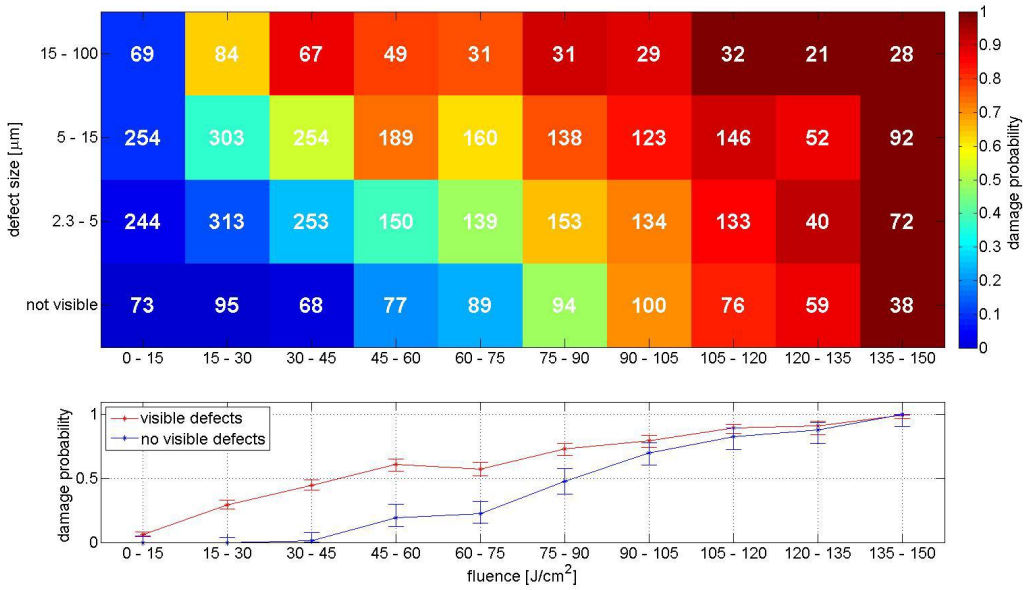

Figure 4. Damage probability map of Set #1 optics (HfO_2/SiO_2 HRs) as a function of fluence and defect size. The color scale encodes probability, and the number in each block is the number of sites tested at that fluence and size.

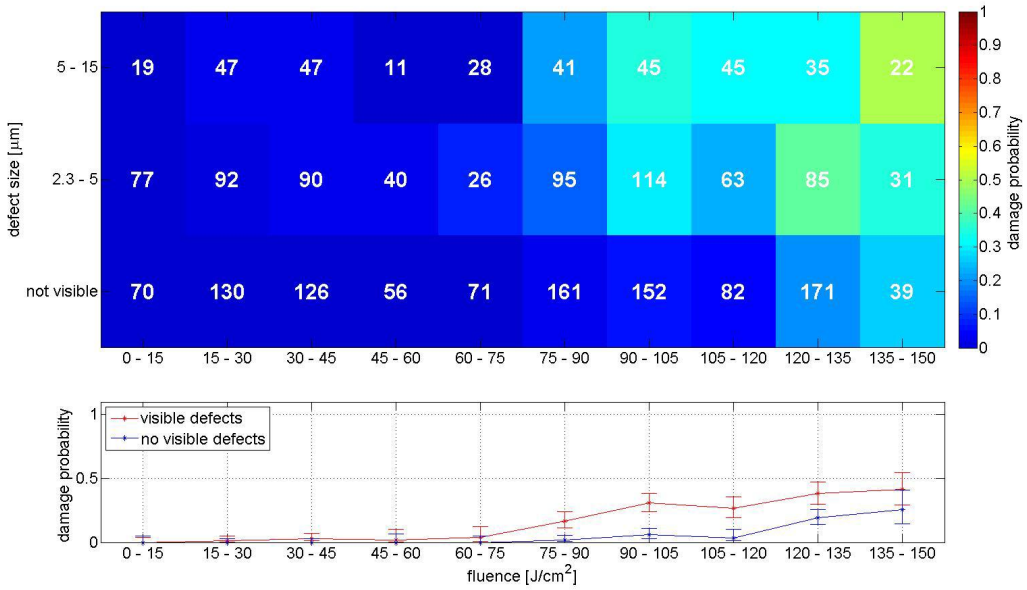

Figure 5. Damage probability map of Set #2 optics (HfO_2/SiO_2 ARs) as a function of fluence and defect size.

The HfO_2/SiO_2 AR data are plotted on the same fluence scale as the HR. The defect size bins are also the same, though without the top-most bin of 15-100 µm simply because there were almost no defects of that size on the AR optics. Note

that there is a real separation of the visible defect and no visible defect damage probability curves, although in this coating they don't begin to split until fluences above about 75 J/cm^2. Unfortunately the 150 J/cm^2 fluence limit of the test system precludes gathering data in the 100% damage probability region.

Figures 6 and 7 are the same kind of damage probability maps for the Set #3 and Set #4 Nb_2O_5/SiO_2 HRs and ARs. The size bins are the same as in the case of the HfO_2/SiO_2 coatings; the fluence scales have been set to show 100% damage probability in each case. The fluence scale only goes up to 30 J/cm^2 for the Nb_2O_5/SiO_2 HRs; by binning in increments of 3 J we still see a low-fluence region from 3 to 12 J/cm^2 in which there is a statistically significant damage probability between the visible defect and no visible defect test sites.

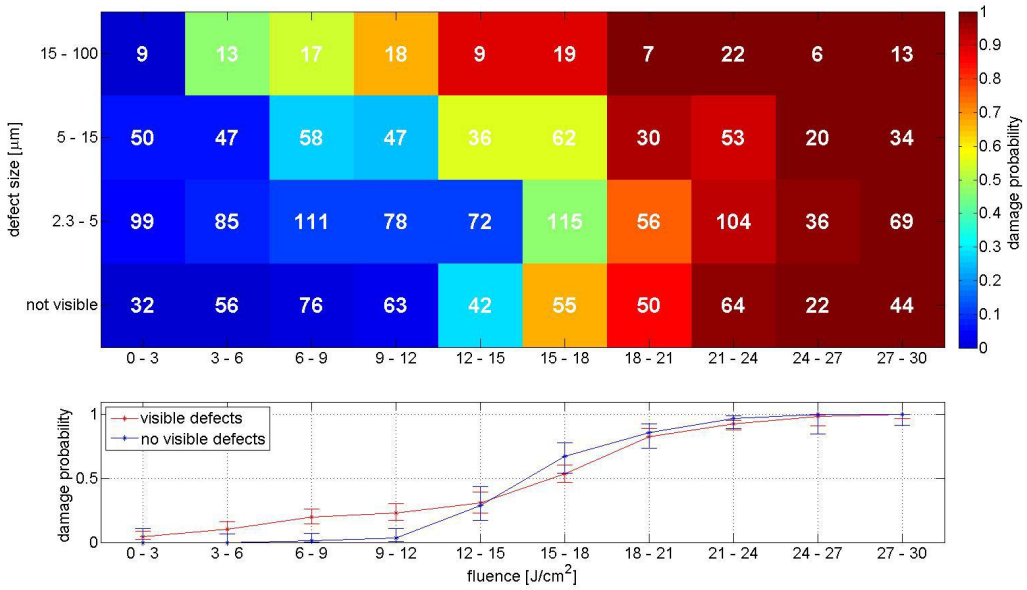

Figure 6. Damage probability map of Set #3 optics (Nb_2O_5/SiO_2 HRs) as a function of fluence and defect size.

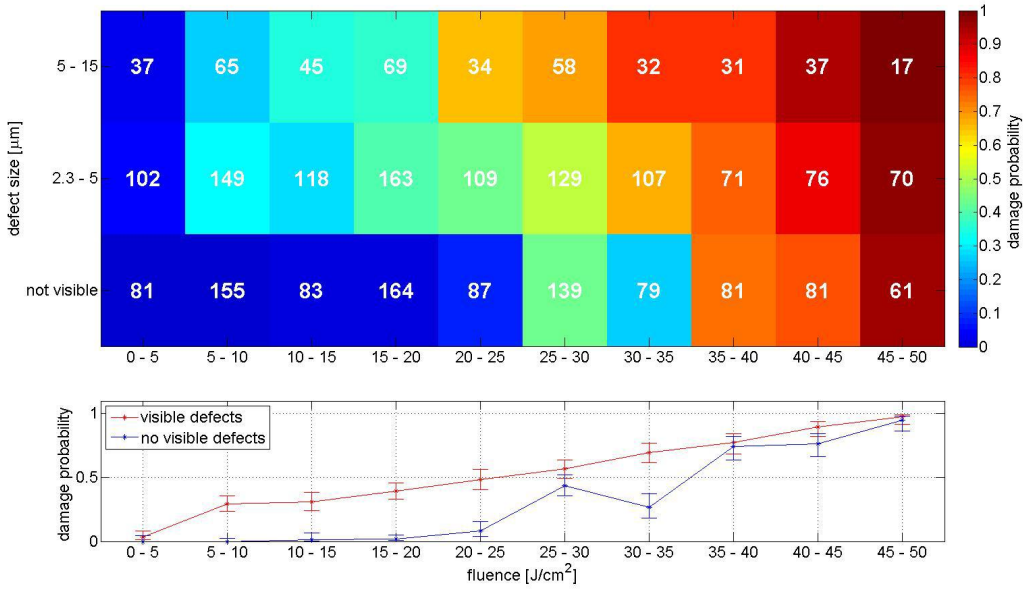

Figure 7. Damage probability map of Set #4 optics (Nb_2O_5/SiO_2 ARs) as a function of fluence and defect size.

The overall behavior of the Nb_2O_5/SiO_2 coatings is very similar to that of the HfO_2/SiO_2 coatings, only shifted lower in fluence by a factor of 3-4. Note that for the Nb_2O_5/SiO_2 material set the AR coatings display a similarly overall greater laser damage resistance compared to the HRs as is seen in the HfO_2/SiO_2 material set, for both the visible defect and no visible defect curves. While it is outside the scope of this paper to address this issue in any detail, we note that one possibility for the difference stems from the electric field distribution in the layers for these particular designs. The maximum field in a high-index layer (where damage is more likely to initiate) in the HR design is larger than that in the AR design. For HfO_2 it is 45% greater; for Nb_2O_5 it is 29% greater.

5. DAMAGE PREDICTION

As stated in the introduction, one of the overarching goals of this research program is to gain some predictive power of laser damage behavior by incorporating knowledge of the thin film designs coupled with a non-destructive surface quality (defect) characterization. When an optic is irradiated there will be some chance of damage due to all visible defects in the beam as well as some possibility of damage even without any visible defects. Let i be an index of the defects, with $i = 0$ defining the no visible defects case; $p_{damage}(s_i;F_i)$ is the experimentally-determined probability of damage as a function of size of defect and fluence, the graphs of which were shown earlier for the four different coating types. The probability that the optic will survive (i.e., no damage will occur) is given by

$$P_{survive} = \prod_{i=0}^{n} \left[1 - p_{damage}\left(s_i ; F_i\right)\right]$$

As an example of how this might be applied, we consider the following hypothetical optic. The coating is an HfO_2/SiO_2 AR, illuminated at a nominal 30 J/cm^2 with the same beam shape as used in the test system. Figure 8 shows the beam profile along with locations of three defects. Table 2 gives the sizes, local fluences, and probabilities of damage associated with each of the defects. The $i = 0$ case is the "background" probability with no visible defects and $F_0 = 30$ J/cm^2. Note that for the HfO_2/SiO_2 AR this happens not to contribute to the likelihood of damage because the no visible defects curve is still zero for this coating type at this fluence (see Figure 5).

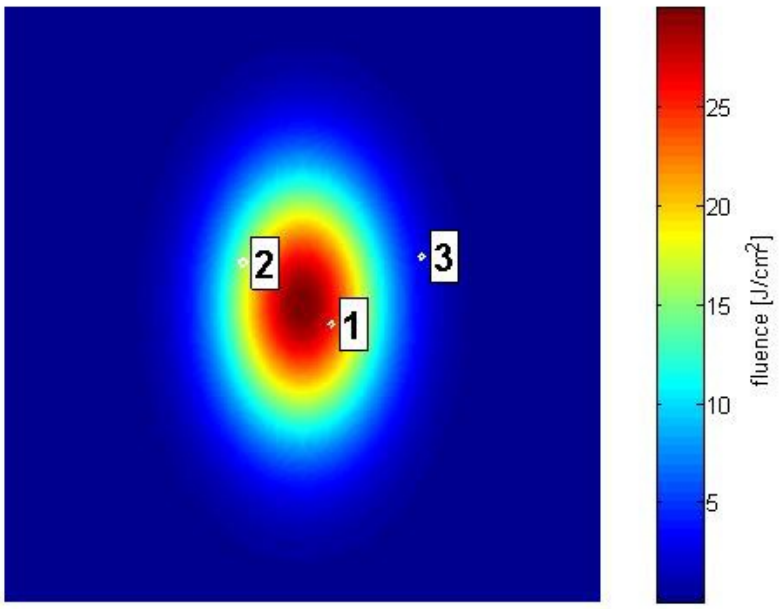

Figure 8. Beam intensity and location of defects for sample damage calculation. The color encodes the local fluence, with a maximum at 30 J/cm^2.

Table 2. List of defect sizes, local fluences, and damage probabilities on hypothetical optic.

i	S_i (µm)	F_i (J/cm^2)	p_{damage}
0	N/A	30	0
1	7.4	26	0.019
2	12	15	0.021
3	8.1	2.8	0

In this case, the calculation indicates that the overall chance of surviving $P_{survive} = 0.96$. Defect #1 is closest to the center of the beam and has a 0.019 chance of causing damage. Defect #2 is farther away and thus experiences a lower local fluence, but its larger size means that its overall chance of causing damage is about the same – 0.021. Defect #3 is so far from the center of the beam that it does not contribute to the overall probability of damage.

6. CONCLUSIONS

A novel laser damage test method using test sites based on the actual measured defect distribution on an optical surface has been developed. This adaptive method has been used to characterize the laser damage behavior of different types of coatings (HR and AR) with different material sets (HfO_2/SiO_2 and Nb_2O_5/SiO_2). This technique allows for discrimination of damage events that are caused by visible pre-existing defects and those that are not. The results indicate a large difference in damage resistance for the two classes of damage events, over a fluence range that is important in the production of commercial laser components. It is likely that defects smaller than 2 µm – below the visibility threshold of this study - play a significant role in the damage at very high fluences.

Follow-on work and improvements to the current technique are foreseen and will proceed along multiple paths. One major effort will be to increase sensitivity using better illumination and light collection, higher resolving power, and a camera with lower noise floor, so that smaller defects can be considered. Another will be to decrease the damaging beam spot size even further, both to avoid defects when desired and reach the higher fluences needed to map out the 100% damage probability area for highly-resistant coatings. Finally, the effectiveness of this technique in predicting damage events for a variety of defect distributions, coating types, and irradiation conditions will be evaluated.

REFERENCES

[1] Bloembergen, N., "Role of cracks, pores, and absorbing inclusions on laser induced damage threshold at surfaces of transparent dielectrics," *Appl. Opt.* 12 (4), 661-664 (1973).

[2] [ISO 21254: Lasers and laser-related equipment – Test methods for laser-induced damage threshold], International Organization for Standardization (2011).

[3] Foltyn, S. R., "Spotsize effects in laser damage testing," Laser Induced Damage in Optical Materials, 1982, 368-379 (1982).

[4] Borden, Michael R., Folta, James A., Stolz, Christopher J., Taylor, John R., Wolfe, Justin E., Griffin, Andrew J., and Thomas, Michael D., "Improved method for laser damage testing coated optics," Proc. SPIE 5591, 59912A-1 – 59912A-8 (2005).

[5] Turner, T., Turchette, Q., and Martin, A. R., "A statistical study of the relationship between surface quality and laser induced damage," Proc. SPIE 8530, 85300R-1 – 85300R-11 (2012).

[6] Richman, S., Martin, A. R., Turchette, Q., and Turner, T., "Method for studying laser-induced damage from sparse defects," Proc. SPIE 8885, 88850H-1 – 88850H-9 (2012).
[7] Turchette, Quentin, and Turner, Trey, "Developing a more useful surface quality metric for laser optics," Proc. SPIE 7912, 791213 (2011).
[8] Turchette, Quentin, and Turner, Trey, "Automated inspection of optics using ISO specifications," Opt. Photonics News, 23(7/8), 14-15 (2012).
[9] Streater, A., and Ness, D. C., "Automated system for laser damage testing of coated optics," Proc. SPIE 5991, 59912B-1 – 59912B-9 (2005).
[10] Guenther, K. H., "Nodular defects in dielectric multilayers and thick single layers," Appl. Opt. 20 (6), 1034-1038 (1981).